Supporting Information for

$Fe^{II}_4L_4$ tetrahedron binds to non-paired DNA bases

Jinbo Zhu,[a] Cally J. E. Haynes,[b] Marion Kieffer,[b] Jake L. Greenfield,[b] Ryan D. Greenhalgh,[a] Jonathan R. Nitschke,[b,*] Ulrich F. Keyser[a,*]

[a] Cavendish Laboratory, University of Cambridge, JJ Thomson Avenue, Cambridge, CB3 0HE, United Kingdom; [b] Department of Chemistry, University of Cambridge, Lensfield Road, Cambridge, CB2 1EW, United Kingdom.

Contents

S1 Synthesis of cage S2

S2 Stability studies of cage 1 using UV-Vis absorption spectroscopy.....S3

S3 Dissociation constants (Kd) determination S5

S4 Fluorescence measurement and melting experiment.....S8

S5 Native polyacrylamide gel electrophoresis (PAGE) S10

S6 Fluorescence lifetime measurement S11

S7 Quenching mechanism S11

S8 Tables S13

References.....S15

S1 Synthesis of cage

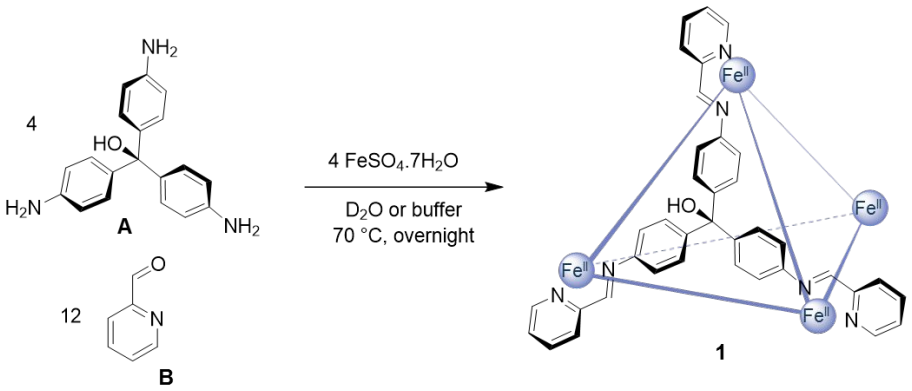

Scheme S1. Subcomponent self-assembly of cage **1** in aqueous solution.

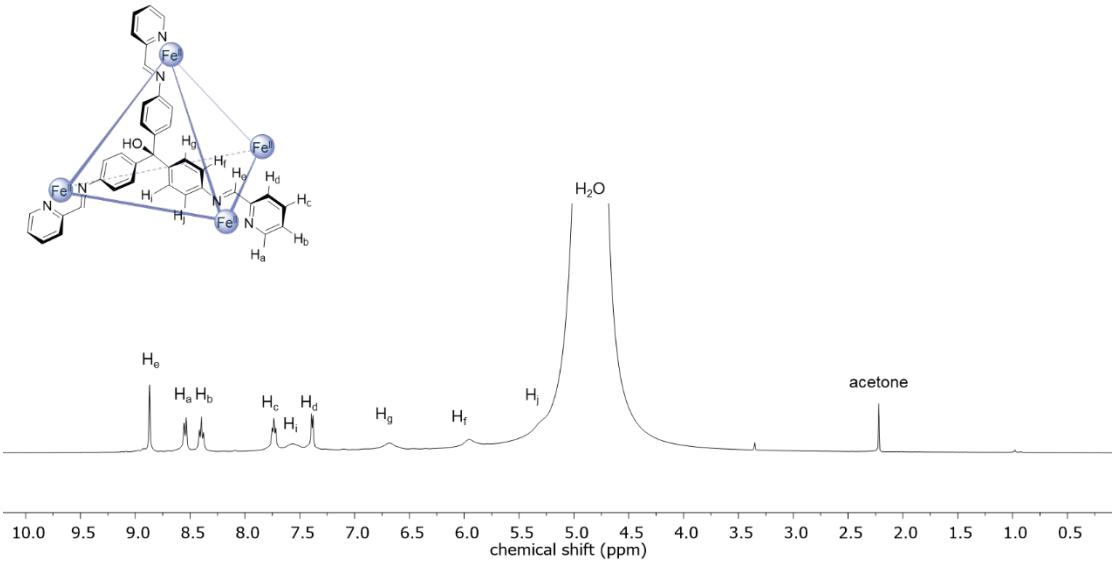

Figure S1. ^{1}H NMR spectrum (400 MHz, 298 K) of 10 mM [**1**]$(SO_4)_4$ in 10 mM PB pH 7.5, 100 mM NaCl, 1:1 H_2O/ D_2O.

Stock solutions of cage **1** were prepared at a concentration of 10 mM and diluted as required. Cage **1** could be synthesized directly in D_2O, 10 mM PB at pH 7.5 (1:1 D_2O/ H_2O) or 10 mM PB with 100 mM NaCl at pH 7.5 (1:1 D_2O/ H_2O) according to the following adapted literature procedure.[1]

As shown in Scheme S1, trianiline **A** (60 mg, 0.2 mmol) and 2-pyridinecarboxalydehyde **B** (57 mL, 64 mg, 0.6 mmol) were dissolved in 5 mL of the desired solvent medium, and the solution was de-gassed with N_2 for 30 min. $FeSO_4.7H_2O$ (54 mg, 0.2 mmol) was added, and the solution was de-gassed for a further 30 min and then heated to 70 °C overnight under N_2. NMR data (Figure S1) was consistent with previously reported data for cage **1** in D_2O.[1]

^{1}H NMR (400 MHz, 298 K, 10 mM PB with 100 mM NaCl at pH 7.5, 1:1 D_2O/ H_2O): δ = 8.87 (s, 12H, H_e), 8.55 (d, J = 7.7 Hz, 12H, H_a), 8.40 (t, J = 7.7 Hz, 12H, H_b), 7.74 (m, 12H, H_c), 7.56 (br. m, 12H, H_i), 7.39 (d, J = 5.6 Hz, 12H, H_d), 6.68 (br. m, 12H, H_g), 5.96 (br. m, 12H, H_f), 5.31 (overlapping with H_2O signal, br. m, 12H, H_j).

S2 Stability studies of cage 1 using UV-Vis absorption spectroscopy

To assess the stability of cage **1** in PBM solution at ambient temperature, a sample of the cage was monitored over time using UV-visible spectroscopy. A spectrum was collected every 30 minutes. Experiments performed at 0.2 μM cage concentration were conducted in a 50 mm pathlength cuvette, and experiments at 4 and 1 μM cage concentration were conducted in a 10 mm pathlength cuvette. To investigate the effect of heating on cage **1** at high temperature in PBM buffer, the absorbance spectra of cage **1** (1 μM) at 80 ℃ was collected every 10 minutes for 3 hours. To investigate the effect of DNA on the stability of the cage, the experiment at 0.2 μM cage concentration was repeated in the presence of 0.1 μM 3WJ. A background spectrum was collected using buffer solution in the same cuvette used for the experiment. The absorbance at 800 nm was set to zero.

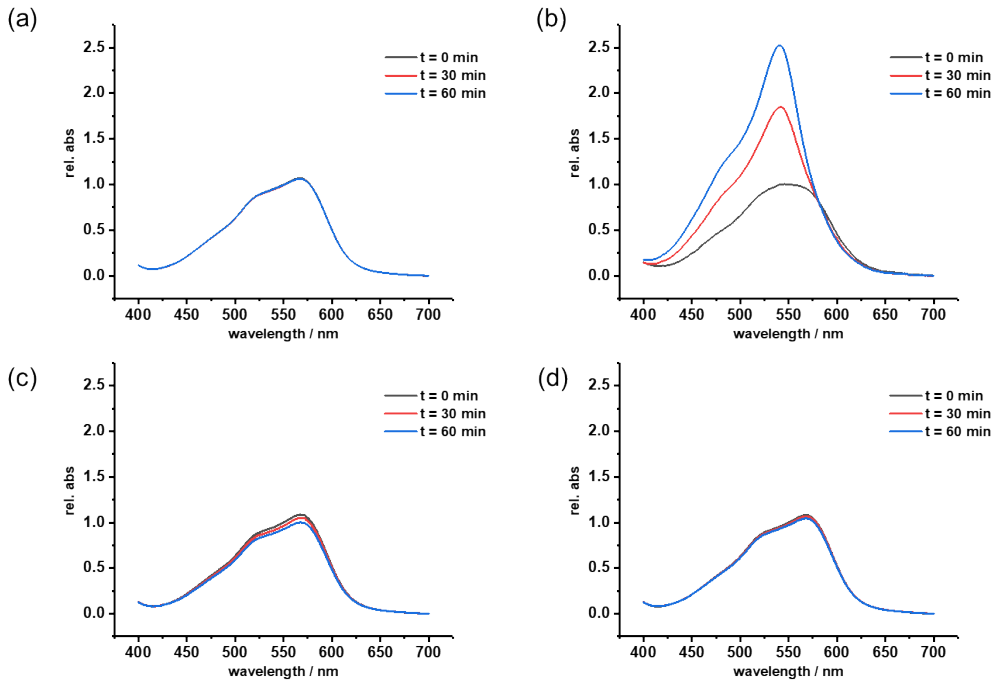

Figure S2 Relative changes to the UV-visible spectrum of cage **1** over the course of 1 hour in PBM between 400 – 700 nm at: (a) [**1**] = 4 μM, room temperature; (b) [**1**] = 1 μM, 80 °C; (c) [**1**] = 0.2 μM, room temperature; (d) [**1**] = 0.2 μM, room temperature, in the presence of 0.1 μM 3wj.

Tracking the potential decomposition of cage **1** was complicated by the strong absorbance profile of pararosaniline **A**[2] (likely a byproduct of cage decomposition), which overlapped with the absorbance of cage **1**. Therefore, we performed a peak deconvolution protocol using Origin 2017 in the absorbance region between 400–700 nm, fitting each band to a Gaussian model (Figure S3a-c). This analysis revealed that initially, the main absorbance in this region consists of 3 bands with absorbance maxima centered at approximately 507, 544 and 577 nm. In each case, an adj. $R^2 > 0.99$ was obtained.

We found that band **c** decayed over the course of the experiment, while bands **a** and **b** were found to increase over time. We therefore concluded that band **c** relates to the MLCT band of cage **1**, while bands **a** and **b** relate to ligand **A** (both when it is a part of cage **1**, and when it has been released as a result of cage decomposition). Therefore, we infer that the decay in peak height band **c** reflects a reduction in the concentration of cage **1**. Hence, we obtained the

decay profiles shown below in Figure S3d.

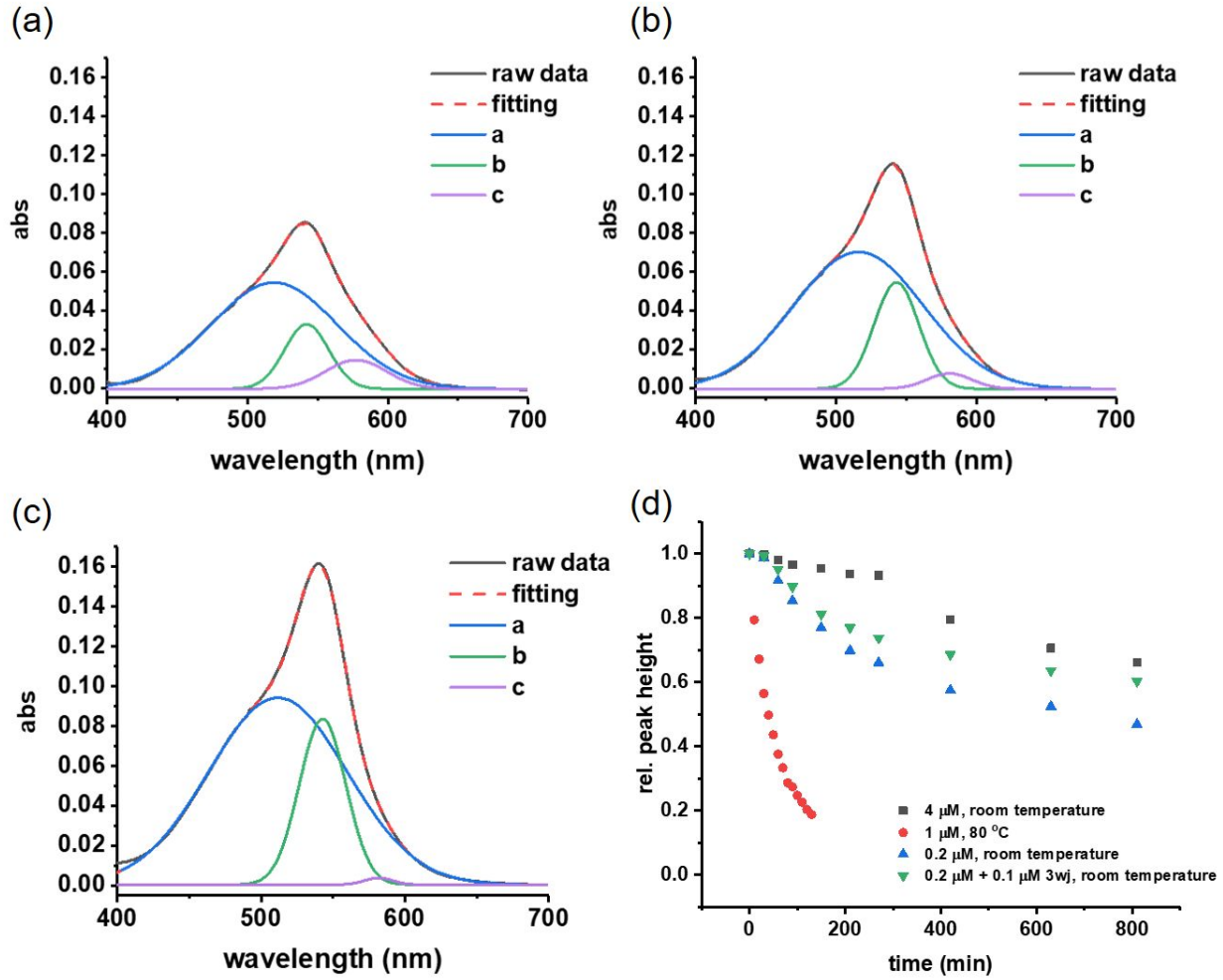

Figure S3. (a-c) Examples of the peak deconvolution analysis from the UV-vis stability study of cage **1** in PBM at 1 μM concentration and 80 °C at different time points: (a) t = 0 min., (b) t = 30 min., (c) t = 60 min. Bands **a** and **b** (shown in blue and green respectively) were found to increase in intensity over time, while peak **c** (shown in purple, assigned as the MLCT band of cage **1**) was found to decrease in intensity over time. (d)The relative change of height of band **c** in the UV-vis stability studies of cage **1** in PBM at various concentrations and temperatures. This data is inferred to be representative of the rate of the decomposition of cage **1**.

Based on these results, we infer that cage **1** shows relatively good stability in PBM at room temperature at 4 μM concentration over a period of hours, and slightly reduced stability over time at 0.2 μM concentration (the lowest cage concentration used in the fluorescence detection studies, Supporting Information S4). It should be noted that the fluorescence detection studies were generally conducted within a timeframe of 10 minutes and cage decomposition is expected to be negligible in this time in both of these cases. The presence of 0.1 μM 3WJ did not decrease the stability of the cage under these conditions.

Cage **1** showed significantly accelerated decomposition at 1 μM concentration when heated at 80 °C, which are the concentration and maximum temperature used in the melting point experiments described in Supporting Information S4. This finding supports our hypothesis that the cage is completely decomposed during the initial heating ramp of the melting point experiments.

S3 Dissociation constants (K_d) determination

The binding between cage and DNA structures (Figure 1b) fits well with 1:1 isotherms (Figure S4), thus one to one binding model as shown in the equilibrium equation below (C refers to cage **1** and D refers to DNA structure) was applied to calculate and compare the dissociate constants (K_d) for different DNA structures.

$$\mathrm{DC} \rightleftharpoons \mathrm{D} + \mathrm{C}$$

For this reaction, the dissociation constant is defined

$$K_\mathrm{d} = \frac{[\mathrm{D}][\mathrm{C}]}{[\mathrm{DC}]}$$

where [D], [C], and [DC] are concentrations of DNA, cage **1** and the complex DNA/**1**, respectively. Binding between the DNA and cage **1** decreases the fluorescence intensity (FI) due to the quenching of FAM modified on DNA by cage **1**, so that the change of the fluorescence reflects the formation of DNA/**1** complex. We introduce the notion of quenching efficiency (QE) to quantify the binding:

$$\mathrm{QE} = \frac{[\mathrm{DC}]}{[\mathrm{D}] + [\mathrm{DC}]} = \frac{I_0 - I}{I_0}$$

where I is the fluorescence intensity of DNA samples with different concentrations of cage **1** and I_0 is the florescence intensity of DNA without cage **1**. We can calculate K_d by plotting the QE versus the concentration of cage **1**. In all the samples, the concentration of DNA was kept at 0.1 μM. According to the following equation

$$\mathrm{QE} = \frac{\mathrm{QE}_{max} \cdot [\mathrm{D}_2]}{K_\mathrm{d} + [\mathrm{D}_2]}$$

where QE_{max} is the maximum QE the cage can reach. We can thus get the value of K_d by fitting the curve of QE=f(concentration) (Figure 1c, Figure S4) to a nonlinear model. The K_d for different DNA structures with **1** are listed in the inset table of Figure 1c.

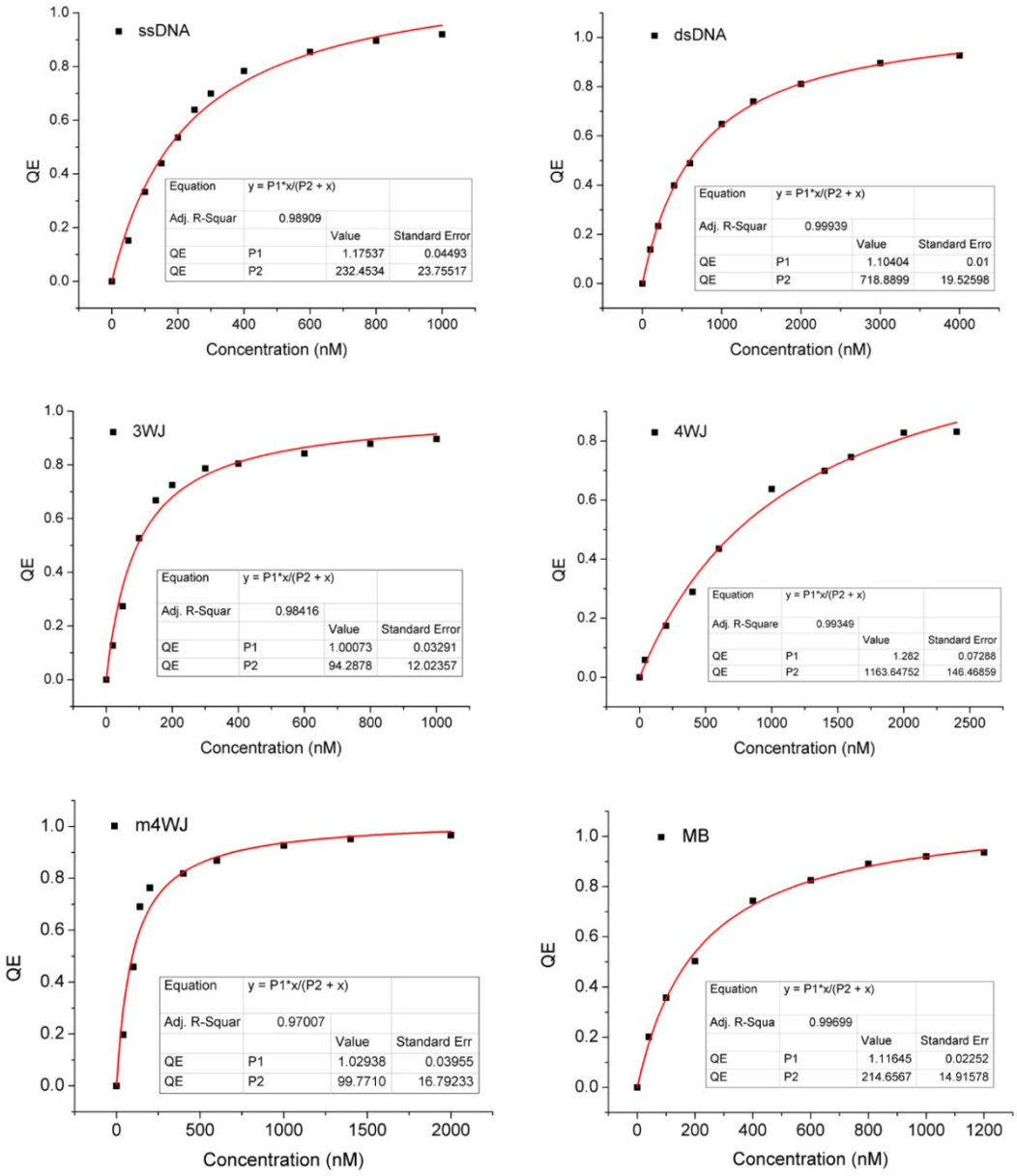

Figure S4. Quenching efficiency (QE) dependency of different DNA structures at varying cage **1** concentrations. All DNA concentrations are 100 nM. The fitting results are shown in the tables.

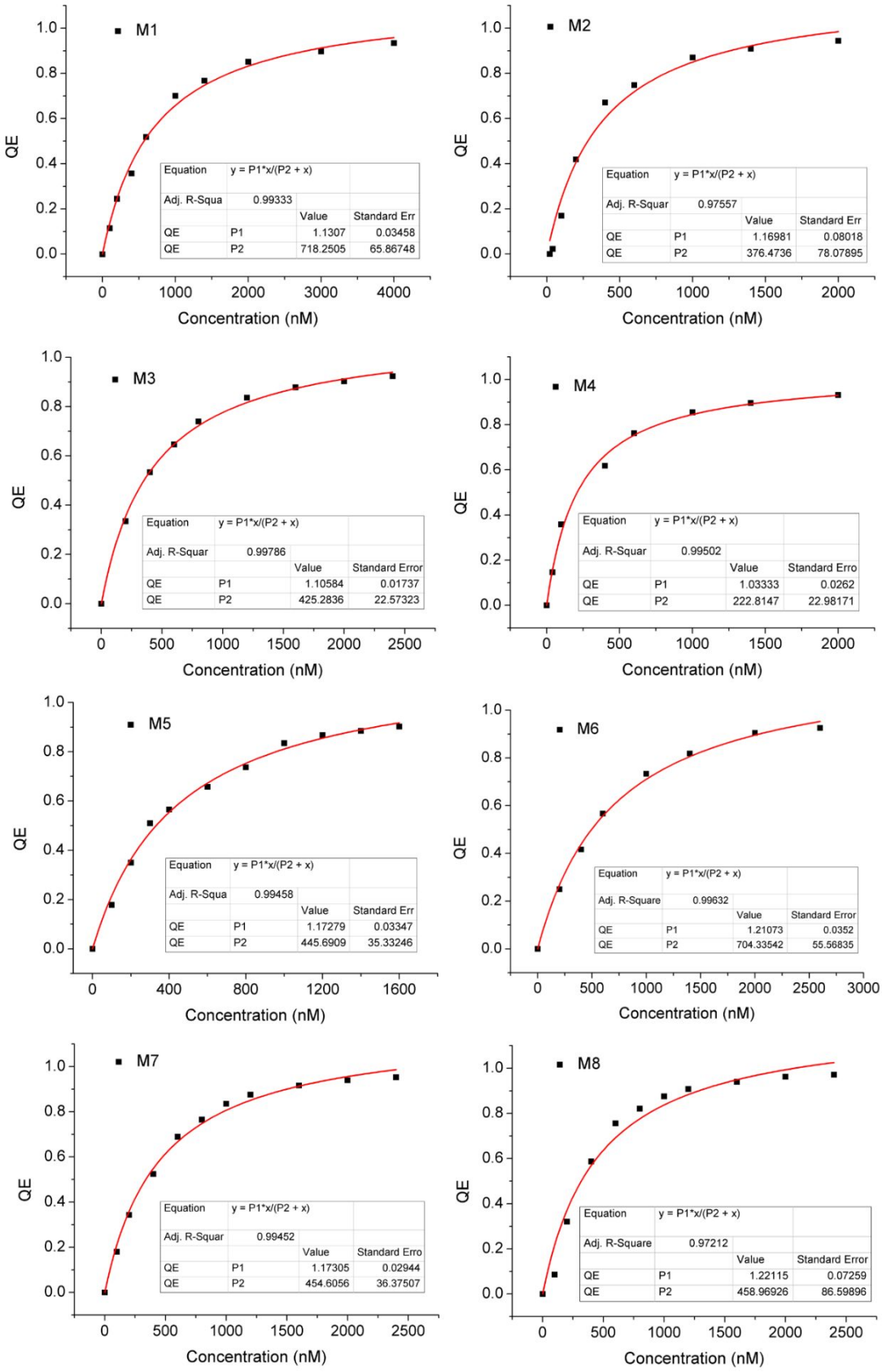

Figure S5. Quenching efficiency (QE) of mismatched dsDNA dependency on cage **1** concentration. All DNA concentrations are 100 nM. The fitting results are shown in the tables.

S4 Fluorescence measurement and melting experiments

DNA oligonucleotides purchased from Integrated DNA Technologies (IDT) were heated at 88°C for 5 min in PBM buffer (10 mM phosphate buffer, 10 mM $MgSO_4$, pH 7.5) and then slowly cooled down to room temperature (20 °C). The strands for folding into the specific DNA structures (i.e. 3WJ, 4WJ) were premixed before heating. Cage **1** diluted to the desired concentration in PBM was added into the DNA solution with a final concentration of 0.2 μM for cage **1** and 0.1 μM for DNA. The mixture was vortexed and the fluorescence emission spectra was collected from 510 nm to 650 nm with an excitation of 495 nm in a 10 mm path-length quartz cuvette using a Cary Eclipse Fluorescence Spectrophotometer (Agilent Technologies, U.S.A.).

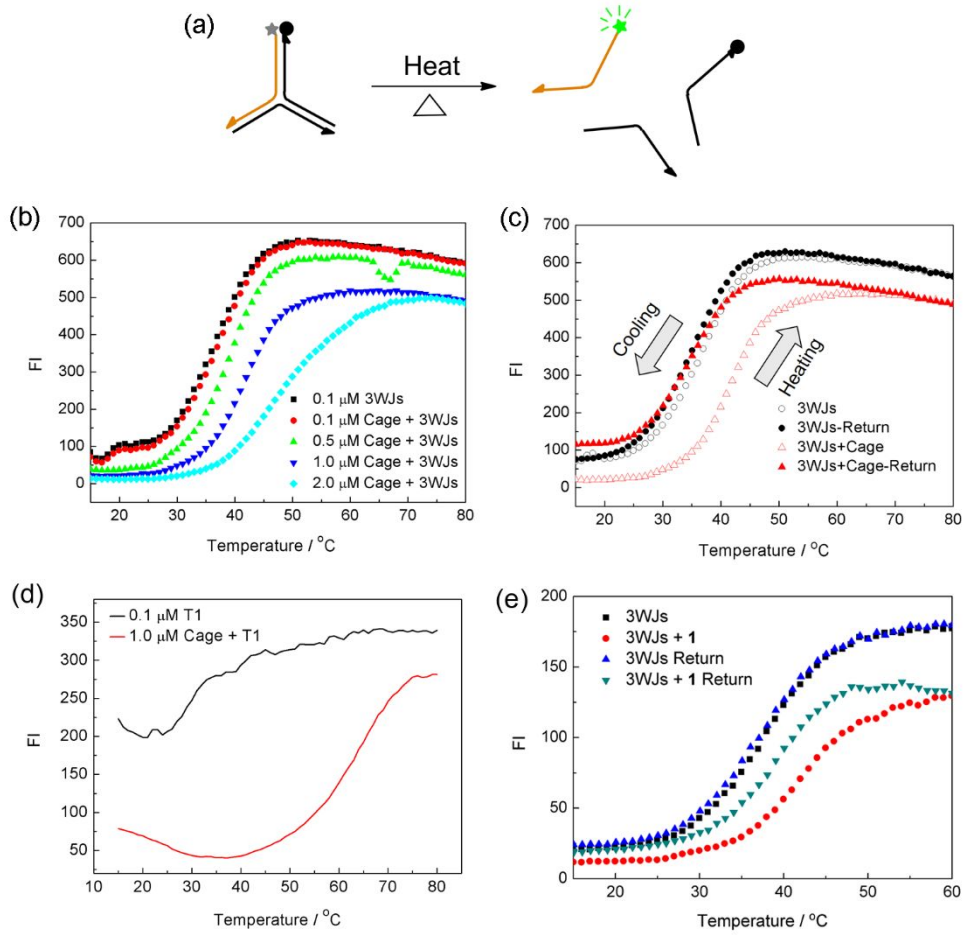

Figure S6. Fluorescence based DNA melting experiments. (a) Schematic diagram for fluorescence based three-way DNA junction melting experiment. (b) Melting curves of 3WJs (0.1 μM) with different concentrations of cage **1**. (c) Fluorescence melting curves of 0.1 μM 3WJs and a mixture of cage **1** (1 μM) and 3WJs (0.1 μM). (d) Melting curve of single strand T1 (0.1 μM) with and without Cage **1** (1 μM). (e) Melting curves of 3WJs (0.1 μM) with and without 1 μM cage **1** from 15 to 60 ℃. Samples were excited at 495 nm and monitored at 520 nm.

We monitored the change in melting temperature (T_m) of the DNA structures after mixing with cage **1** to investigate the strength of this interaction. We hypothesized that cage **1** may stabilize the DNA structure and thus lead to a higher T_m. The high absorbance of the cage and its ligands below 300 nm prevented us from following the change in absorbance of the DNA by UV-vis and circular dichroism spectroscopy. Therefore, we employed fluorescence

spectroscopy (Figure S6a) to obtain the melting curves. Since **1** decomposed above 80 °C (Figure S3), the 3WJ DNA was redesigned using shorter strands (3WJs, Table S1) for a lower T_m. In melting experiments monitored through fluorescence, the solution was heated from 15 to 80 °C and returned to 15 °C at a rate of 0.25 °C/min in a 10 mm path-length cuvette to disassemble the 3WJs. Mineral oil was added on top of the solutions to avoid evaporation. The samples were excited at 495 nm and fluorescence emission intensity at 520 nm were recorded every degree centigrade. We infer the resulting increase in fluorescence intensity to result from the release of the fluorescent-labeled strand from the 3WJs during the melting process.

A cage concentration dependent *Tm* increase phenomenon was observed in Figure S6b. In Figure S6c, when 1 μM cage **1** was added to 0.1 μM 3WJs, a 5 °C shift to a higher T_m was observed in the melting curve. On the return cooling ramp, however, no effect of cage **1** on the thermal fluorescence response was observed. We infer that this is due to the disassembly of cage **1** at higher temperatures, as was observed in the absence of DNA (Figure S2). We thus infer that the fragments of **1**, resulting from cage disassembly, do not affect the fluorescence and the stability of 3WJs, as anticipated from the results of control measurements involving these fragments (Figure S10c).

Although a shift of 5 °C in the melting curve is observed upon addition of 1 μM cage **1** (Figure S6c), it is challenging to entirely ascribe the higher *Tm* to the cage binding. Our control experiment in Figure S6d indicates cage **1** still survives around the DNA melting temperature (42 °C), because the fluorescence of the ssDNA with cage **1** is not completely recovered until 75 °C. Thus, the cage may still quench the fluorescence of the released ssDNA at this temperature and lead to a higher melting temperature. The fluorescence melting experiment was repeated in a narrow temperature range from 15 to 60°C in Figure S6e. The 3WJs/cage **1** return curve lay between 3WJs and the mixture heating up curve, which meant cage **1** partly decomposed at temperature up to 60 °C.

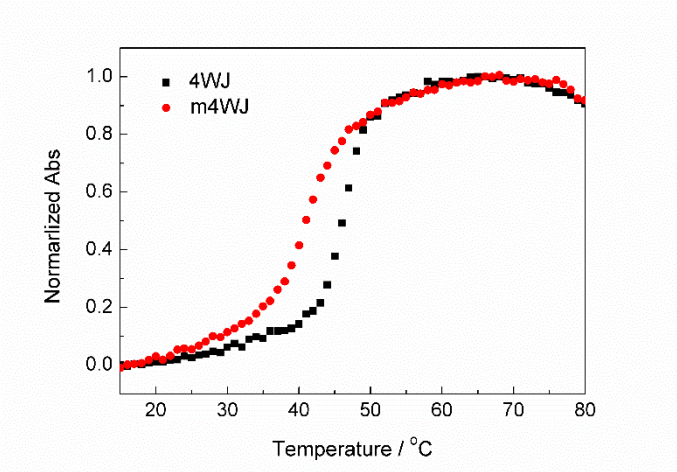

Figure S7. UV melting curves of 1 μM 4WJ and m4WJ in PBM buffer. Thermal melting was monitored at 260 nm. DNA solution was heated from 15 °C to 80 °C at a rate of 0.25 °C/min in a 10 mm path-length cuvette. Mineral oil was added on top of the solutions to avoid evaporation.

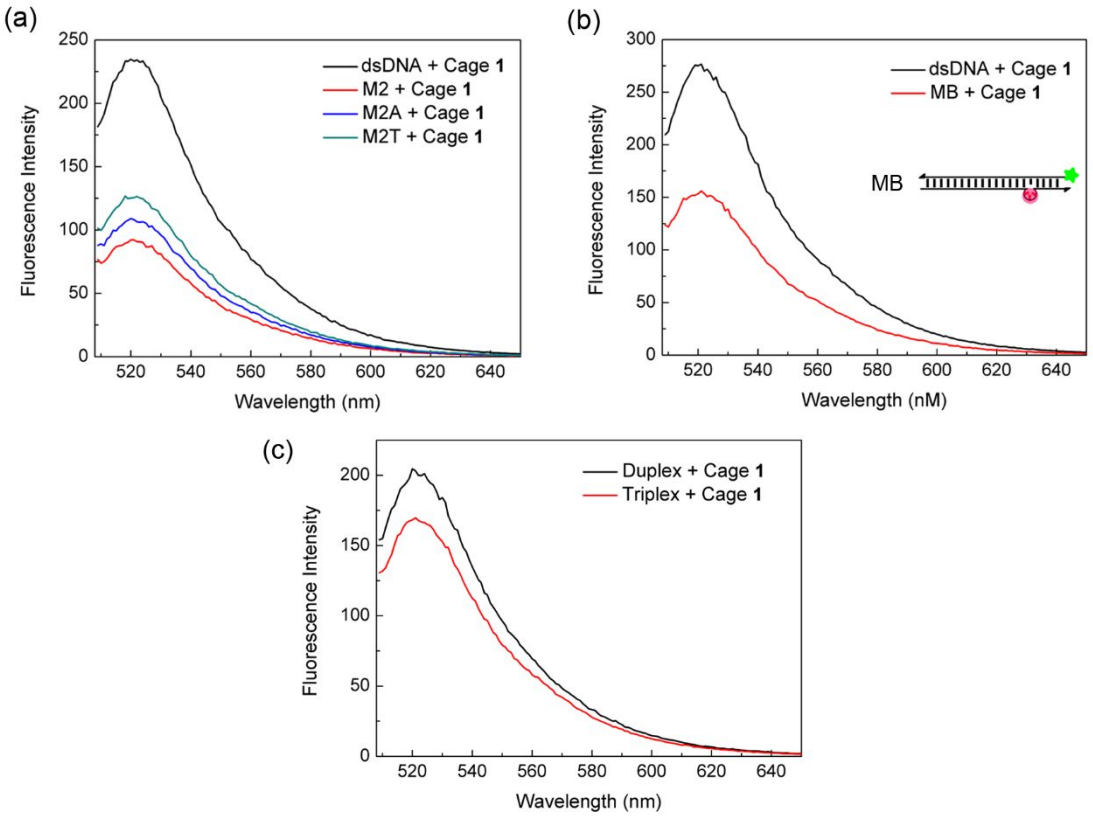

Figure S8. Effect of 0.2 μM cage **1** on the fluorescence of 0.1 μM dsDNAs sequences with (a) different base mismatches and (b) bulge. (c) Effect of 0.2 μM cage **1** on the fluorescence of 0.1 μM duplex and triplex in PB-Ag buffer (10 mM PB, 100 mM $NaNO_3$, 10 μM $AgNO_3$, pH 7.5). Ag^+ was added to stabilize the DNA triplex structure in neutral solution.[9]

Mismatches of different base pairs were compared in Figure S8a. As shown in Table S1, strand MS2A and MS2T were used to generate two mismatched dsDNA M2A and M2T. Compared with GG base mismatch in M2, GA and GT base mismatches in M2A and M2T were also detectable by cage **1**, respectively.

Interaction between bulged DNA and cage **1** was investigated in Figure S8b. Based on the design of M1, mismatched G base was replaced by three A bases to form the bulged DNA MB. The fluorescence quenching is obviously enhanced three unpaired A bases.

As an important DNA structure, triplex DNA (Table S1, DT1-3) is also investigated here. Since most triplexes are only stable in acidic condition such as CG.C+ triplets, 10 μM AgNO3 was added into the buffer to assist the formation of triplex DNA in neutral solution.[9] In Figure S8c, as we expected the fluorescence intensity of the cage **1**/triplex mixture is very close to the cage**1**/duplex, so the cage is not sensitive to the triplex.

S5 Native polyacrylamide gel electrophoresis (PAGE)

DNA samples in PBM buffer were heated at 88 °C for 5 min and then slowly cooled to room temperature before PAGE analysis. Cage **1** (50 μM) was added into DNA (5 μM) and then mixed with 6 × loading buffer before loaded into 15% native polyacrylamide gel. In Figure 2b, the 3WJ was annealed in PBM at the concentration of 2 μM and diluted to 1 μM to load into the gel. The electrophoresis was conducted in 1 × TB buffer (89 mM Tris, 89 mM boric

acid, 10 mM $MgSO_4$, pH 8.0) at constant voltage of 110 V (10 V cm^{-1}) for 1.5 hour. The gel was stained for 20 min in GelRed (from Biotium, Inc.) then visualized on a UV transilluminator.

S6 Fluorescence lifetime measurements

Time-correlated single photon counting (TCSPC) fluorescence-lifetime imaging microscopy (FLIM) was conducted on a custom-built rig. The microscope used a pulsed supercontinuum laser (FianiumWhiteLase, Fianium Ltd., Southampton, UK) for excitation with a 40 MHz repetition rate and a spectrum ranging from 400 to 2400 nm. The source beam was passed through a cold mirror to remove infrared radiation above 700 nm. Wavelengths below 700 nm were then passed through an acousto-optic tunable filter (AOTF, AA Opto-electronic AOTFnC-VIS) where the modulation frequency was tuned electronically in Lab-View. The excitation wavelength was selected to be 480 nm for 6-FAM modified 3WJ samples with a bandwidth of 1 – 2 nm. The beam was then passed through a filter wheel with a band-pass (474/27 nm). A neutral density filter was then used to control the beam intensity. The beam was then passed into the confocal scan unit (Olympus Fluoview FV300) towards the sample via a 20/80 broad bandwidth beam splitter. The beam splitter reflected 20 % of the excitation light on to the sample and 80 % of the fluorescence signal towards the confocal pinhole. The fluorescence signal was then directed into a filter wheel with band-pass filter (525/39 nm) towards a high speed photomultiplier tube (PMT, PMC-100, Becker & Hickl GmbH, Berlin, Germany). The photon count rates were maintained below 1 % of the repetition rate and images were acquired over 250 s. TCSPC FLIM images were analysed using FLIMfit (version 5.1.1, Imperial College London). Monoexponentials and biexponential decays were fitted to the lifetime curves. 80 µL samples of 1 µM 3WJ with or without 2 µM cage **1** were pipetted onto glass coverslips (Menzel, borosilicate glass, 24 × 50 mm) under ambient conditions during imaging and the instrument response function (IRF) was measured on a blank coverslip.

S7 Quenching mechanism

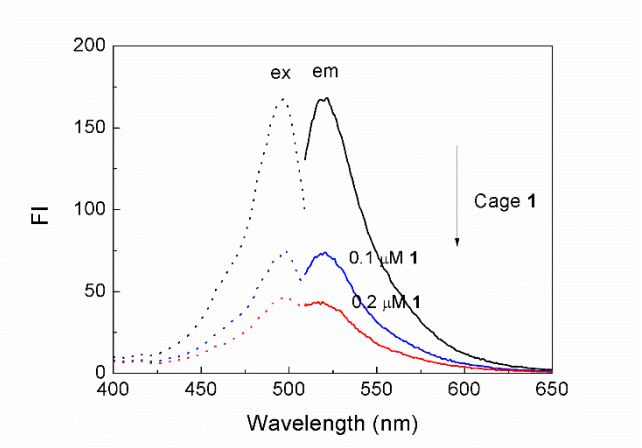

Figure S9. Emission (solid line) and excitation (dash line) spectra of 3WJ (0.1 µM) with increasing concentration of cage **1**.

There are two modes of quenching: static and dynamic. In static quenching, a new ground-state complex will be formed, which usually results in a detectable change of the excitation spectrum. However, the addition of cage **1** did not change the maximum excitation wavelength of FAM labelled on 3WJ (Figure S9), which means no new complex is formed. Thus, static quenching was ruled out.

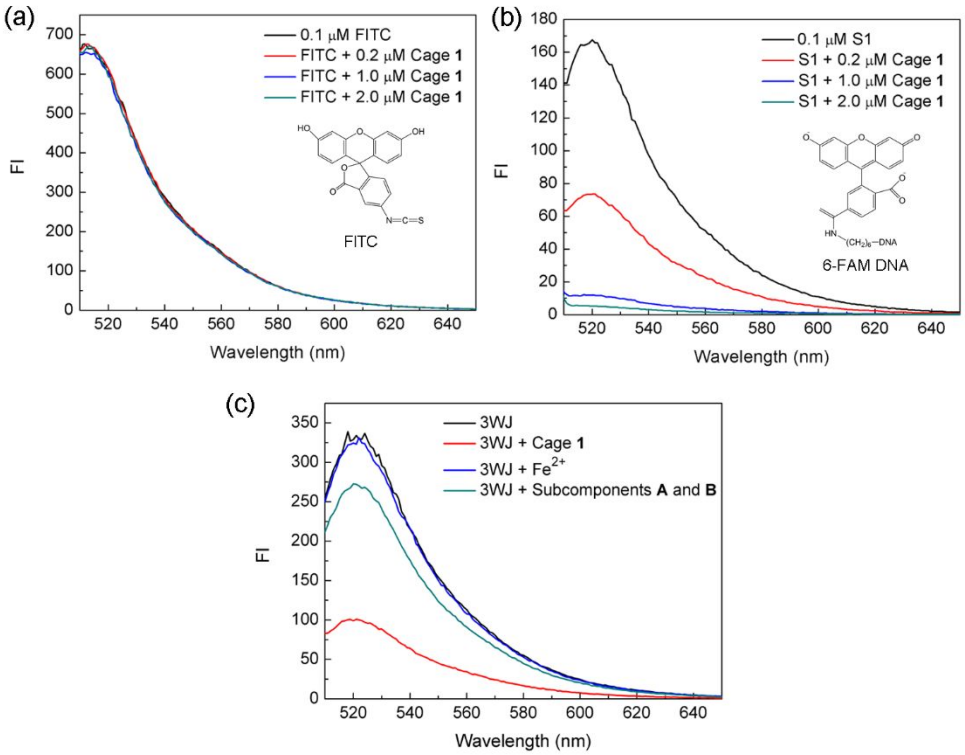

Figure S10. Effects of cage **1** on the fluorescence intensity (FI) of (a) FITC and (b) 6-FAM labeled ssDNA (0.1 μM, DNA strand S1, Table S1). (c) Effects of the precursors of cage **1** on the fluorescence of 3WJ (0.1 μM). Cage **1** (0.2 μM), equivalent concentrations of $FeSO_4$ (0.8 μM) and a mixture of cage subcomponents **A** (0.8 μM) and **B** (2.4 μM), as shown in Scheme S1, were separately mixed with 3WJ.

Dynamic quenching encompasses several quenching mechanisms, including collision quenching, energy transfer and electron transfer. Collision quenching is excluded, because the fluorescence of FITC (a FAM analogue, Figure S10a) remained the same when cage **1** was in solution (Figure S10a) without DNA. If the quenching had been caused by intermolecular collisions of dye and cage **1**, DNA would not play a role in the quenching.

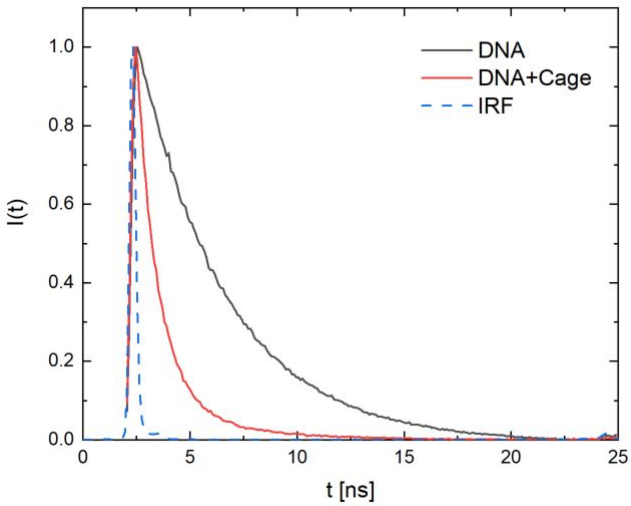

Figure S11. Lifetime fits for 1 μM DNA (3WJ) (black), 1 μM DNA (3WJ) + 2 μM cage **1** (red), and instrument response function (IRF, blue dashed). The red curve yields a faster drop off than the black curve, suggesting that the

fluorescence lifetime of the dyes on DNA with cage **1** is shorter. DNA alone (black curve) shows a monoexponential decay with a lifetime of 4.15 ns, addition of the cage leads to a biexponential decay with a mean lifetime of ~ 1.1 ns (τ_1 ~ 4.44 ns, τ_2 ~ 0.785 ns, β_1 ~ 0.077, β_2 ~ 0.923).

Fluorescence resonance energy transfer (FRET) is another possible reason for the cage induced quenching, because the absorption of cage **1** from 400-600 nm does overlap with the emission spectrum of FAM and a clear decrease of the fluorescence lifetime induced by cage **1** was observed in Figure S11. However, as shown in Table S2, when we tested the other dyes modified on ssDNA (listed at the end of Table S1), cage **1** failed to effectively quench some of them (Cy3 and TAMRA) while the maximum emission wavelengths were still overlapping with the absorption spectrum of the cage. Additionally, FRET quenching efficiency is expected to exhibit a dependence on separation distance with an inverse 6th-power law, but in stark contrast Figure 3a shows a good linear relationship from 2.7 nm to 6.8 nm.

Finally, photoinduced electron transfer (PET) mechanism is the remaining mechanism, because cage **1** demonstrated a similar quenching characteristic as observed for guanine bases in DNA strands (which is based on PET mechanism) for a range of different fluorescent labels.[3] In addition, the photoexcited Fe^{II} center in cage **1** may act as an electron donor to excited dyes, in similar fashion to guanine.[4] However, PET normally happens over a short range (less than 1 nm), which is inconsistent with the linear distance response observed in Figure 3a. Since the cage can also quench the fluorescent label on duplex DNA to some extent (Figure 1b) and the length of the linker between the FAM and the DNA and the flexibility of the DNA strand (especially the longest one) are not taken into account, these background factors will affect our results by rendering the quenching mechanism more difficult to elucidate. Thus, further study will be required in order to understand the mechanism, particularly in light of the linear relationship between distance and fluorescence response, which is not consistent with the hypotheses we currently have. We infer the cage-based fluorescence quenching mechanism to result from a combination of or competition between different quenching processes.[5]

S8 Tables

Table S1.[a] Sequences of DNA strands used in this work.

DNA name	Strand name	Sequence
ssDNA	S1	FAM- TGAGGATGTGTAGGTTGATG
dsDNA	S1	FAM- TGAGGATGTGTAGGTTGATG
	S2	CATCA ACCTACACATCCTCA
3WJ	S1	FAM- TGAGGATGTGTAGGTTGATG
	S3	CATCAACCTAAGAATGAGAC
	S4	GTCTCATTCTCACATCCTCA
3WJs	T1	FAM- TGAGGATG GACAGCA
	T2	TGCTGTC TGTAGGT
	T3	ACCTACA CATCCTCA – IBFQ
4WJ	S1	FAM- TGAGGATGTGTAGGTTGATG
	S3	CATCAACCTAAGAATGAGAC
	S5	GTCTCATTCTAGTACATGTG

	S6	CACATGTACTCACATCCTCA
m4WJ	S1	FAM- TGAGGATGTGTAGGTTGATG
	S7	CATCAACCT*TT*GAATGAGAC
	S5	GTCTCATTCTAGTACATGTG
	S6	CACATGTACTCACATCCTCA
3WJ-8	L1	TCTGTATGGGATTTTGCTAAACAACTTTCAACTAGTATCGTTC GGACATGT-FAM
	L2	ACATGTCC TCACTTCTGTG
	L3	CACAGAAGTGA GAACGATACTAGTTGAAAGTTGTTTAGCAAAATCCCATACAGA
3WJ-11	L1	TCTGTATGGGATTTTGCTAAACAACTTTCAACTAGTATCG TTCGGACATGT-FAM
	L4	ACATGTCCGAA TCACTTCTGTG
	L5	CACAGAAGTGA CGATACTAGTTGAAAGTTGTTTAGCAAAATCCCATACAGA
3WJ-14	L1	TCTGTATGGGATTTTGCTAAACAACTTTCAACTAGTA TCGTTCGGACATGT-FAM
	L6	ACATGTCCGAACGA ACACTTCTGTG
	L7	CACAGAAGTGT TACTAGTTGAAAGTTGTTTAGCAAAATCCCATACAGA
3WJ-17	L1	TCTGTATGGGATTTTGCTAAACAACTTTCAACTA GTATCGTTCGGACATGT-FAM
	L8	ACATGTCCGAACGATAC ACACTTCTGTG
	L9	CACAGAAGTGT TAGTTGAAAGTTGTTTAGCAAAATCCCATACAGA
3WJ-20	L1	TCTGTATGGGATTTTGCTAAACAACTTTCAA CTAGTATCGTTCGGACATGT-FAM
	L10	ACATGTCCGAACGATACTAG ACACTTCTGTG
	L11	CACAGAAGTGT TTGAAAGTTGTTTAGCAAAATCCCATACAGA
M1	S1	FAM- TGAGGATGTGTAGGTTGATG
	MS1	CATCAACCTACACAT*G*CTCA
MB	S1	FAM- TGAGGATGTGTAGGTTGATG
	MA3	CATCAACCTACACAT*AAA*CTCA
M2	S1	FAM- TGAGGATGTGTAGGTTGATG
	MS2	CATCAACCTACACATCCT*G*A
M2A	S1	FAM- TGAGGATGTGTAGGTTGATG
	MS2A	CATCAACCTACACATCCT*A*A
M2T	S1	FAM- TGAGGATGTGTAGGTTGATG
	MS2T	CATCAACCTACACATCCT*T*A
M3	S1	FAM- TGAGGATGTGTAGGTTGATG
	MS3	CATCAACCTACACATCCTC*T*
M4	S1	FAM- TGAGGATGTGTAGGTTGATG
	MS4	CATCA ACCTACACATCCT*GT*
M5	S1	FAM- TGAGGATGTGTAGGTTGATG
	MS5	CATCA ACCTACACAT*GG*TCA
M6	S1	FAM- TGAGGATGTGTAGGTTGATG
	MS6	CATCA ACCTACA*GT*TCCTCA
M7	S1	FAM- TGAGGATGTGTAGGTTGATG
	MS7	CATCA ACCTAC*TGT*TCCTCA
M8	S1	FAM- TGAGGATGTGTAGGTTGATG
	MS8	CATCA ACCTA*GTGT*TCCTCA
Duplex	DT1	GAG AGG AGA GAG AAG AGG AAG

	DT2	FAM- CTT CCT CTT CTC TCT CCT CTC
Triplex	DT1	GAG AGG AGA GAG AAG AGG AAG
	DT2	FAM- CTT CCT CTT CTC TCT CCT CTC
	DT3	CTC TCC TCT CTC TTC TCC TTC
FAM-DNA		FAM- TGAGGATGTGTAGGTTGATG
TET-DNA		TET- TGAGGATGTGTAGGTTGATG
HEX-DNA		HEX- TGAGGATGTGTAGGTTGAGGAGTGATG
Cy3-DNA		Cy3-TGATGAGTTGGATTGATGTG
TAMRA-DNA		TAMRA-AGAGAGTAGGTAGGTGAAGGAGTGATG
Cy5-DNA		Cy5-AGGTGAGGTAGTTGAGTAGT

[a] All sequences start from the 5' end.

Table S2. Quenching efficiency of cage **1** for different dyes attached to ssDNA (Table S1). Concentrations for cage **1** and ssDNA are 0.1 μM and 0.2 μM, respectively.

Modified dye	Ex/Em (nm)	Quenching ratio[a]
6-FAM	495/520	69 %
TET	522/539	85%
HEX	538/555	86%
Cy3	550/564	15%
TAMRA	559/583	21%
Cy5	648/668	32%

[a] Quenching ratio = $(FI_{DNA}-FI_{DNA\text{-}cage})/FI_{DNA}$, where FI_{DNA} and $FI_{DNA\text{-}cage}$ are the fluorescence intensity of the DNA sample with and without cage **1**, respectively.

Table S3. K_d values of 3WJ/cage **1** and other 3WJ binders previously reported.

3WJ binder	Cage **1**[a]	Triptycene **1** [6],a	1,5-BisNP-O[7],b	2,7-BisA-O[7],b	3,3'-TrisBP[7],b	Cationic calix[3]carbazole[8],a
K_d/μM	0.094	0.221	0.021	0.00053	0.26	23.1

[a] Calculated based on fluorescence assay; [b] calculated based on ESI-MS assay.

Table S4. K_d values of different DNA structures with cage **1** obtained from Figure S4 and S5.

DNA	ssDNA	dsDNA	3WJ	4WJ	m4WJ	M1	M2	M3	M4	M5	M6	M7	M8	MB
K_d/μM	0.23	0.72	0.094	1.2	0.10	0.72	0.38	0.43	0.22	0.45	0.70	0.46	0.46	0.21

References

[1] Bilbeisi, R. A.; Clegg, J. K.; Elgrishi, N.; de Hatten, X.; Devillard, M.; Breiner, B.; Mal, P.; Nitschke, J. R. Subcomponent self-assembly and guest-binding properties of face-capped Fe4L4(8+) capsules. *J. Am. Chem. Soc.* **2012,** *134* (11), 5110-5119.

[2] Kosanić, M. M.; Tričković, J. S. Degradation of pararosaniline dye photoassisted by visible light. *J. Photoch. Photobio. A* **2002,** *149* (1), 247-251.

[3] (a) Edman, L.; Mets, U.; Rigler, R. Conformational transitions monitored for single molecules in solution. *Proc. Natl. Acad. Sci.* **1996**, *93*, 6710-6715; (b) de Silva, A. P.; Moody, T. S.; Wright, G. D. Fluorescent PET (Photoinduced Electron Transfer) sensors as potent analytical tools. *Analyst* **2009**, *134*, 2385-2393.

[4] (a) Torimura, M.; Kurata, S.; Yamada, K.; Yokomaku, T.; Kamagata, Y.; Kanagawa, T.; Kurane, R. Fluorescence-Quenching Phenomenon by Photoinduced Electron Transfer between a Fluorescent Dye and a Nucleotide Base. *Anal. Sci.* **2001**, *17*, 155-160; (b) Seidel, C. A. M.; Schulz, A.; Sauer, M. H. M. Nucleobase-Specific Quenching of Fluorescent Dyes. 1. Nucleobase One-Electron Redox Potentials and Their Correlation with Static and Dynamic Quenching Efficiencies. *J. Phys. Chem.* **1996,** *100* (13), 5541-5553.

[5] (a) Haenni, D.; Zosel, F.; Reymond, L.; Nettels, D.; Schuler, B. Intramolecular Distances and Dynamics from the Combined Photon Statistics of Single-Molecule FRET and Photoinduced Electron Transfer. *J. Phys. Chem. B* **2013,** *117* (42), 13015-13028; (b) Stewart, M. H.; Huston, A. L.; Scott, A. M.; Oh, E.; Algar, W. R.; Deschamps, J. R.; Susumu, K.; Jain, V.; Prasuhn, D. E.; Blanco-Canosa, J.; Dawson, P. E.; et al. Competition between Förster Resonance Energy Transfer and Electron Transfer in Stoichiometrically Assembled Semiconductor Quantum Dot–Fullerene Conjugates. *ACS Nano* **2013,** *7* (10), 9489-9505.

[6] Barros, S. A.; Chenoweth, D. M. Recognition of Nucleic Acid Junctions Using Triptycene-Based Molecules. *Angew. Chem., Int. Ed.* **2014,** *53* (50), 13746-13750.

[7] Duskova, K.; Lamarche, J.; Amor, S.; Caron, C.; Queyriaux, N.; Gaschard, M.; Penouilh, M.-J.; de Robillard, G.; Delmas, D.; Devillers, C. H.; Granzhan, A.; Teulade-Fichou, M.-P.; Chavarot-Kerlidou, M.; Therrien, B.; Britton, S.; Monchaud, D. Identification of Three-Way DNA Junction Ligands through Screening of Chemical Libraries and Validation by Complementary in Vitro Assays. *J. Med. Chem.* **2019,** *62* (9), 4456-4466.

[8] Yang, Z.; Chen, Y.; Li, G.; Tian, Z.; Zhao, L.; Wu, X.; Ma, Q.; Liu, M.; Yang, P. Supramolecular Recognition of Three Way Junction DNA by a Cationic Calix[3]carbazole. *Chem.–Eur. J.* **2018,** *24* (23), 6087-6093.

[9] (a) Feng, L.; Huang, Z.; Ren, J.; Qu, X. Toward site-specific, homogeneous and highly stable fluorescent silver nanoclusters fabrication on triplex DNA scaffolds. *Nucleic Acids Res.* **2012,** *40* (16), e122; (b) Ihara, T.; Ishii, T.; Araki, N.; Wilson, A. W.; Jyo, A. Silver Ion Unusually Stabilizes the Structure of a Parallel-Motif DNA Triplex. *J. Am. Chem. Soc.* **2009,** *131* (11), 3826-3827.